Hot Gas Environment Around STOVL Aircraft in Ground Proximity—Part 1: Experimental Study

R. MacLean,* J. Sullivan,† and S. N. B. Murthy‡
Purdue University, West Lafayette, Indiana 49707

In connection with the problems of the ingestion of exhaust gases of engines in V/STOL and STOVL aircraft in ground effect, an experimental investigation was conducted on a typical model configuration using marker nephelometry to establish the interactions between the jets, forward velocity, and the ground. The test rig consisted of a two inlet configuration with four low subsonic velocity jets impacting vertically on a flat plate; the vertical distance between the plate and model undersurface was adjustable. A wind tunnel provided forward airflow to simulate landing into a wind with a velocity that could be set at 0–0.1 times the jet velocity. A videotape of concentration distribution revealed several vortical features in the interaction region, which were affected variously by the distance between the ground plane and model and the inlet suction. The frame-averaged data compared favorably with time-averaged predictions carried out elsewhere in a companion investigation. However, such predictions did not seem to reveal several aspects of the vortical flow features that should affect instantaneous distortion into the engine inlet.

I. Introduction

THE ingestion of hot exhaust gases into engine inlets in ground effect is an important consideration in the design and operation of V/STOL and STOVL aircraft. Such ingestion leads to a time varying rise in inlet temperature in addition to velocity and stagnation pressure distortion in the inlet flow. The performance of the engine is affected in a variety of ways, including compressor stall. Ingestion is an extremely complex process influenced by the aircraft's altitude, attitude, velocity, and geometry. The flowfield around the aircraft that arises from these conditions is complex and unsteady, which increases the difficulty in determining the causes of hot gas ingestion. Considerable effort has gone into analyzing and predicting the overall flowfield in the past.[1-5] Nevertheless, important questions remain.

One of the principal questions in hot gas ingestion concerns the time varying distortion in the flow and thermal fields at the inlet face. Consider the landing, for example, of a V/STOL aircraft. It is of considerable interest to establish the manner in which instantaneous distortion varies during approach of the aircraft to the landing ground. One approach to addressing that problem is to examine if there are any discernible characteristic features in the flow interaction region beneath the aircraft and, further, if there is a pattern to changes in such characteristic features as the aircraft descends as a function of time. This has been one of the main motivations in the current investigation.

In a concurrent, companion investigation,[6] an investigation was carried out on predicting the interactive flowfield. The calculations were based on time-averaged and Reynolds-averaged equations of motion. A second motivtion for the current investigation at Purdue University was to provide experimental data for comparison with those predictions.

In the experiments, a nonintrusive technique, marker nephelometry, was chosen to determine the flowfield, qualitatively and also quantitatively, around a four-jet, two-inlet V/STOL aircraft model in ground effect. Details on the use of marker nephelometry and the method of quantifying the flow visualization data can be found in Refs. 7 and 8. Based on the visualization of the (smoke) concentration field, one could obtain the flow interactions. At the same time, the concentration field is analogous to the temperature field, provided the concentration and the temperature are both in the nature of a marker, neither introducing density nor transport differences in the flowfield. On this basis, the concentration field determined in the experiments became available for comparison with predictions of the temperature field reported in Ref. 6.

The three main geometric parameters in this experiment were H, the model height above the ground plane, D_j, the jet diameter, and H_I, the inlet height above the ground. The main velocity parameters are U, the freestream velocity, and V_j, the jet velocity. The scaling parameters, although given in terms of D_j and V_j, are essentially unknown.

The flow velocities, both of the jet and of the forward wind, have small subsonic values in the current experiments. Compressibility effects are therefore entirely eliminated. At the same time, it may be worth pointing out that, although the ratio of jet to forward wind velocities is typical of ground effect situations, the absolute velocity of the jet is too small for direct comparison of observed flowfield interactions with those found in practice. Nevertheless, it is hoped that the nature of flow interactions may be adequately representative of those occurring in actual aircraft operations.

In the following sections, details of the experiments and the data obtained are presented along with 1) various observations on the structure of the flow interaction region and 2) some typical comparisons between experimental data and predictions. Regarding the first, a videotape forms the principal basis of observations.

The formation of various vortical structures in the flowfield is one of the most noticeable features. In particular, three types of vortex structures may be identified: 1) the horseshoe ground vortex, 2) the forward vortex pair, and 3) the vortices associated with the interaction between the fountain and the jets. These vortex structures are influenced by changes in the freestream velocity, model height above the ground plane, model geometry, and inlet suction.

The horseshoe ground vortex is shown in Fig. 1. It forms in the ground plane and occurs in the region where boundary-layer flow produced by the jets impacting on the ground plane

Presented as Paper 90-2269 at the AIAA/SAE/ASME/ASEE 26th Joint Propulsion Conference, Orlando, FL, July 16–18, 1990; received Aug. 16, 1990; revision received Dec. 6, 1990; accepted for publication Dec. 12, 1990.

*Graduate Student, School of Aeronautics and Astronautics. Student Member AIAA.
†Professor, School of Aeronautics and Astronautics. Member AIAA.
‡Professor, School of Mechanical Engineering. Member AIAA.

meets the freestream flow. It has the features of a horseshoe vortex, although it will be split by the forward motion of the flow emanating from the inner flow region between the pair of forward jets.

The forward vortex pair is also shown in Fig. 1. Each of the two counter-rotating vortices in the forward vortex pair are anchored to the ground plane, generally with their axes oriented normal to the ground plane. The forward vortex pair is located in the stagnation region where the flow moving radially outward from between the two forward jets and the freestream flow meet. The unsteady nature of the forward vortex pair makes it difficult to determine the various factors contributing to its formation.

The third major feature visible in the flowfield is a pair of counter-rotating vortices between a side pair of jets and the fountain, as shown in Fig. 2. At high velocity ratios, only the downstream vortex seems to be formed. This feature propagates outward from the region between the jets crosswise into the freestream flow. In this region, only the downstream vortex is visible in smoke concentration measurements.

II. Experimental Apparatus

The model, shown in Fig. 3, has four jets and two inlets, with the jet centerlines aligned with the inlet centerlines. It has the same dimensions, relative to the jet diameter, as those used in the example of predictions carried out by Van-Overbeke and Holdeman.[9] The jet diameter (D_j) of the test model is 0.5 in., whereas that employed in Ref. 9 is roughly 1.5 in.; accordingly, all of the other dimensions of the test configuration have been scaled by the factor 0.333 relative to that of Ref. 9. The jet velocity of the model was nominally set at 75 ft/s, yielding a Reynolds number of about 20,000 based on the jet diameter. Larger mass flow rates and thus jet velocities decreased the smoke concentration in the flowfield to unusable amounts. Each of the four half-inch jets was preceded by a contraction section. A set of screens and honeycomb just before the contraction were utilized to remove large-scale unsteady features in the flow. The inlet was located 5 in., or 10 jet diameters, forward from the front pair of jets, measured from the jet centerlines. The inlet measured 0.5 in. horizontally by 1.0 in. vertically, with the bottom of the inlet 0.25 in. from the base of the model from which the jets emanated. The distance between the ground and inlet, denoted H_I, was then 0.25 in. greater than the distance between the model and ground plane.

Figure 4 shows the complete experimental setup. The model was mounted in a small two-dimensional wind tunnel with an open section. A fan upstream of the model provided an airflow to simulate wind past the model in forward motion. A set of two screens and a honeycomb and a two-to-one contraction were utilized in this flow to remove most of the swirl and nonuniformity. The tunnel section measured 22 in. horizontally and 12 in. vertically. The maximum velocity of airflow that could be generated was about 7.5 ft/s. This gave freestream-to-jet velocity ratios of up to 0.10. The mean velocity of the wind tunnel varied by about ±5% across the test section.

The model was mounted in the test section with the jets pointing up toward a 30 in. by 30 in. glass ground plate serving as the ground plane in the test section. This resulted in a less complicated mounting and support structure for the model. The distance between the model and the ground plane could be adjusted over a distance between 0 and 14 jet diameters.

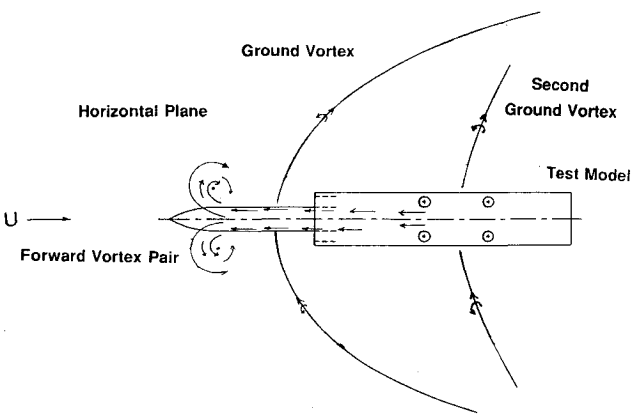

Fig. 1 Illustration of ground vortex and forward vortex pair.

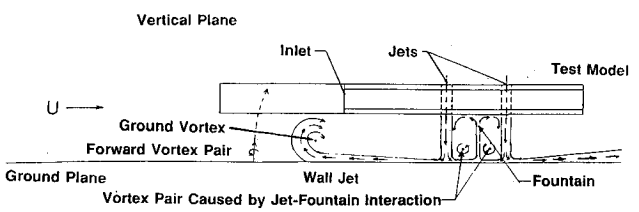

Fig. 2 Illustration of vortex pair produced by jet-fountain interaction.

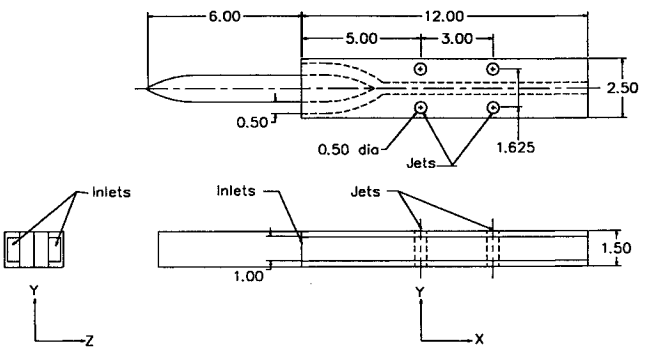

Fig. 3 Test model.

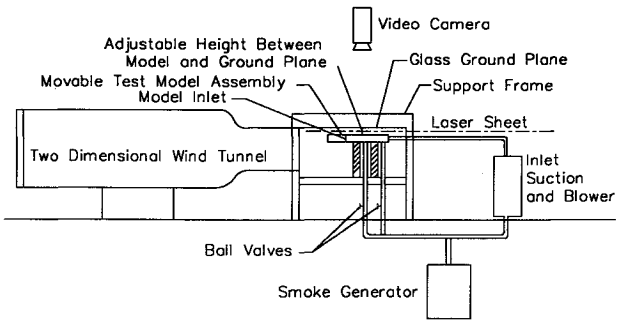

Fig. 4 Experimental setup.

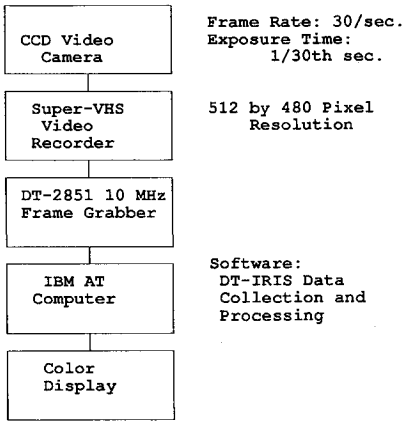

Fig. 5 Data acquisition flow chart.

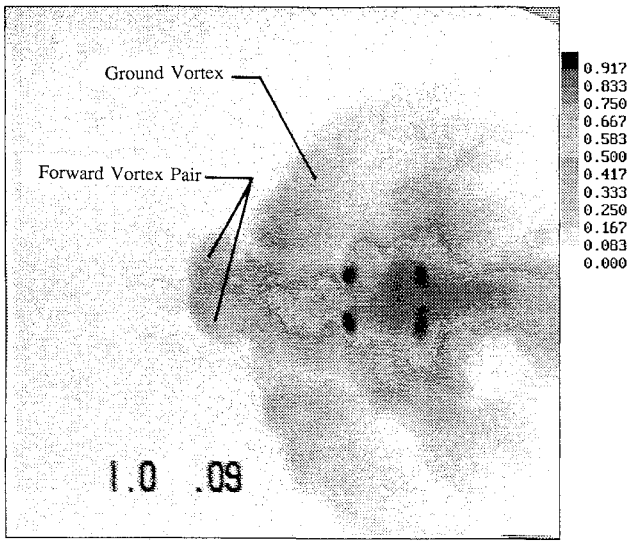

Fig. 6 Single frame of smoke concentration at midplane: $H/D_j = 4$, $U/V_j = 0.09$.

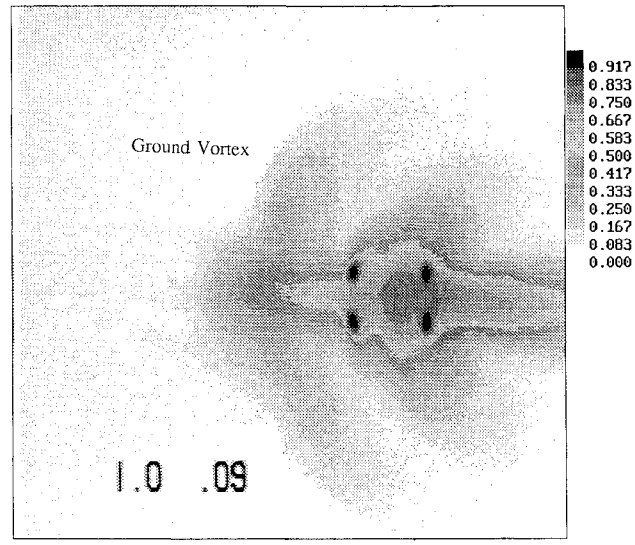

Fig. 8 127 frame average of smoke concentration at midplane: $H/D_j = 4$, $U/V_j = 0.09$.

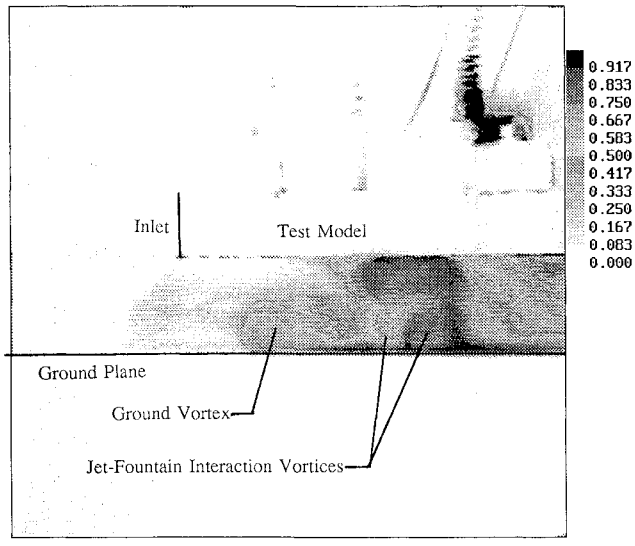

Fig. 7 Single frame of smoke concentration with vertical laser sheet: $H/D_j = 4$, $U/V_j = 0.09$.

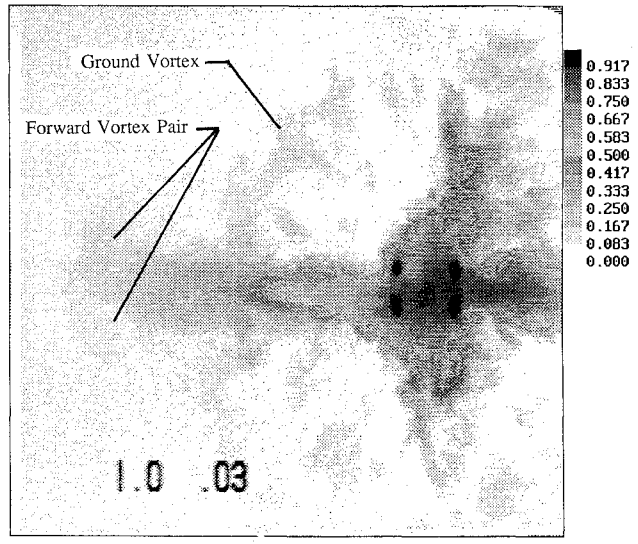

Fig. 9 Single frame of smoke concentration at midplane: $H/D_j = 4$, $U/V_j = 0.03$.

A single blower was utilized to supply air to the jet nozzles. The inlet to the blower was connected to the model inlets that merged into a single duct. In this manner, the inlet and the jet mass flows were essentially balanced. The velocity of each of the jets was controlled by means of a ball valve. An oil mister was used to generate smoke particles of propylene glycol. The smoke was injected between the blower and ball valves. Four feet of 1.25 in. diameter tubing were incorporated between the crossflow smoke injector location and the jets to provide adequate mixing distance. Except for a small proportion of the larger particles that tended to condense on the tubing walls, the low velocity in the tubing assured that the smoke was reasonably well mixed with air at entry to the jet.

A laser sheet was used to illuminate the smoke particles in the flowfield. The laser sheet was generated using a 5W argon-ion laser and a cylindrical lens that could be rotated to create a horizontal (x-z plane) or vertical (x-y plane) laser sheet. The cylindrical lens and laser were mounted on a movable table, allowing the laser sheet to illuminate different planes. Three-dimensional pictures of the flowfield could then be generated by combining several different planes of data, although they are not being presented here.

Figure 5 shows the data acquisition flow chart. A video camera was mounted to take pictures of the illuminated smoke particles in the flowfield. The shutter speed of the camera was 1/30th of a second. The images were sent to a Super VHS videorecorder, stored on videotape, and then sent to a Data Translation high-speed frame grabber. The frame grabber was capable of capturing an image at a sampling frequency of 10 MHz, giving the image a screen resolution of 512 horizontal by 480 vertical pixels. Eight-bit analog-to-digital conversion allowed up to 256 different concentration levels. The output of the frame grabber could then be averaged and stored on an IBM computer for later processing. Both single frames and 127-frame averages of the flowfield were stored on the computer. The frame grabber could also be used to redisplay false color images (lower amplitude features in blue and higher amplitude features in red in the current case) in real time to a display or other videorecorder. Images stored on the IBM computer were processed by generating line plots of concentration X or concentration Z. Grey scale images of the flowfield could also be generated.

III. Results

The flowfield around the model has a number of interesting features. These are illustrated in a series of cases with relevant images of the flowfield extracted from the videotape. It may be worth pointing out that the videotapes illustrate clearly

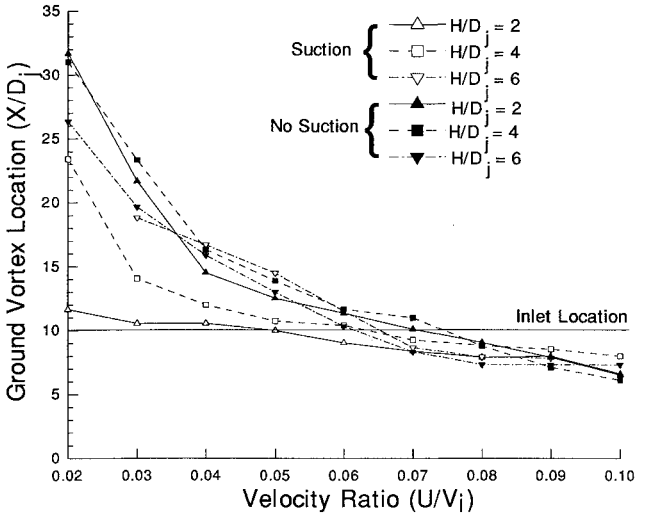

Fig. 10 Distance from front jet pair to ground vortex location vs velocity ratio (U/V_j).

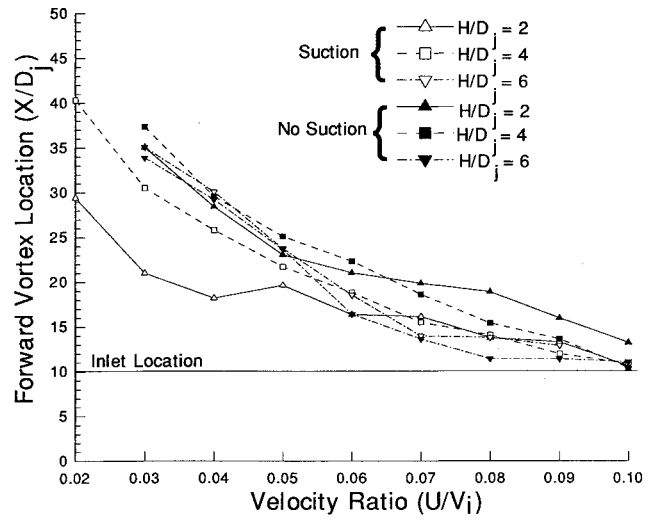

Fig. 11 Distance from front jet pair to forward vortex pair location vs velocity ratio (U/V_j).

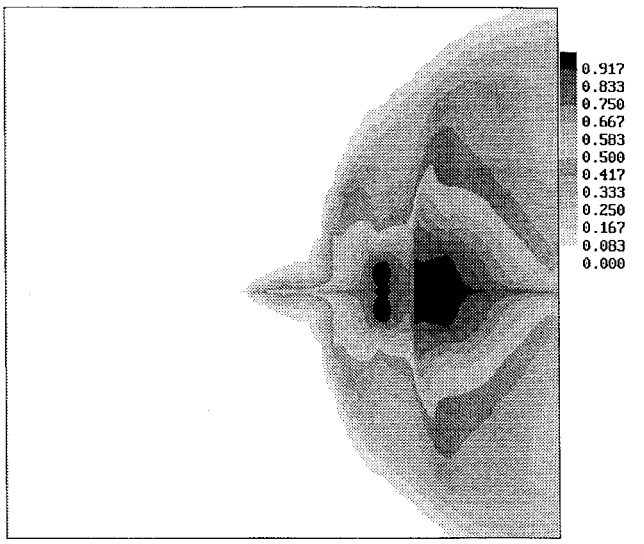

Fig. 12 Numerical temperature profile at ground plane: H/D_j = 4, U/V_j = 0.09.

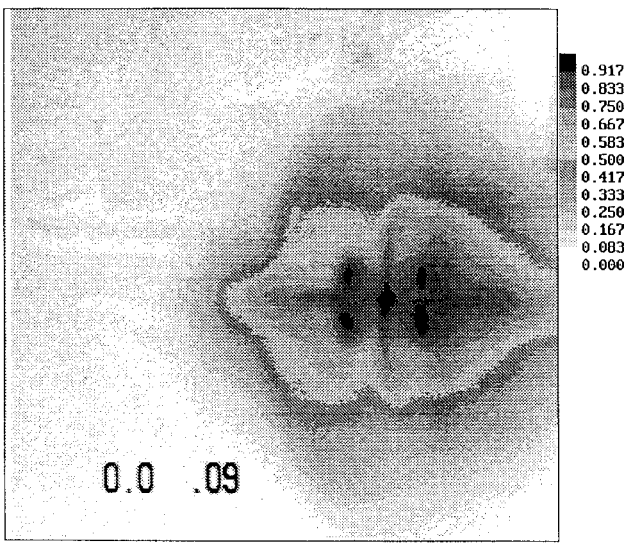

Fig. 13 Experimental smoke concentration at ground plane: H/D_j = 4, U/V_j = 0.09.

both the unsteadiness of the flowfield as well as the shifting asymmetries in the formation and location of vortical entities.

In the following, we first illustrate the formation of the three main types of vortical structures. The presence of such structures is somewhat blurred in frame averaging. Next, the influence of the velocity ratio and inlet suction on the location of the ground vortex and forward vortex pairs are illustrated both qualitatively and quantitatively. Finally, a comparison is provided between the experimental data and predictions from Ref. 6.

A. Vortical Structures in the Flowfield

Figure 6 shows two of the features in an image of the smoke concentration in the flowfield. The velocity ratio U/V_j is 9.09, and the model is four jet diameters above the ground plane. For this case, the laser sheet is positioned two jet diameters above the ground plane. One of the two features shown is the formation of the horseshoe ground vortex in the ground plane. A cross section of the vortex can be seen in profile in Fig. 7. It has been seen in experiments by Colin and Olivari[10] investigating single jets in cross flows. This feature has also been seen in operations with the Harrier. Unlike the single jet case, where one obtains a continuous horseshoe vortex, the ground vortex is bisected in the four poster case by flow moving radially outward along the stgnation line (or the center line) between the two forward jets. The behavior of the two branches of the ground vortex in relation to the outward flow between the jets is then determined by the ratio U/V_j.

The second major feature visible in Fig. 6 is the pair of vortices referred to as the forward vortex pair, formed where flow moving radially outward along the stagnation line between the two forward jets meets the freestream flow. This feature is located in the stagnation region of the two flows. The forward vortex pair is normal to the ground plane and is found to be unsteady in the videotape, with the size and location of each vortex changing rapidly.

The third feature, caused by interactions between the fountain and jets, can be seen in Fig. 7. This feature is caused by the impingment of the fountain on the model and entrainment of the resulting flowfield by the jets. This is evident as two counter-rotating vortices between the jets and fountain. These two vortices propagate out of the inner flow region between the jets crosswise into the freestream flow, where at least the downstream vortex is distinctly visible in the x-y plane both in time-averaged and single frames of the flowfield.

Figure 8 shows a 127-frame average of the flowfield shown earlier in Fig. 6. The forward vortex pair and the ground vortex have become smeared.

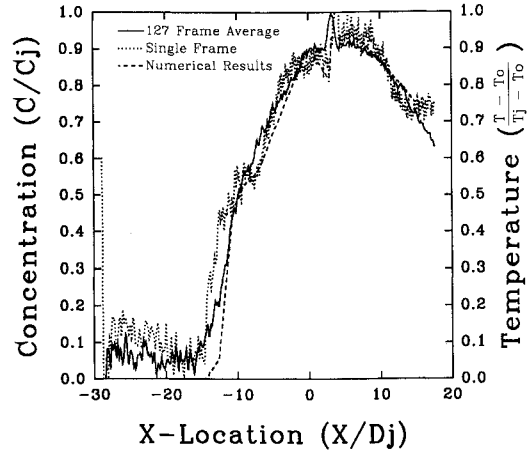

Fig. 14 Numerical and experimental results at ground plane: profile through model centerline, $H/D_j = 4$, $U/V_j = 0.09$.

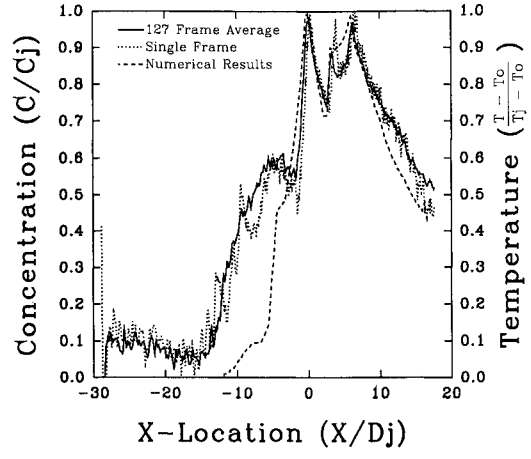

Fig. 15 Numerical and experimental results at ground plane: profile through left jet pair centerline, $H/D_j = 4$, $U/V_j = 0.09$.

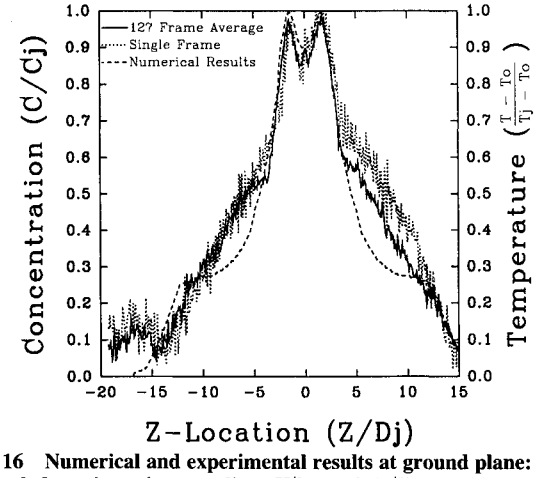

Fig. 16 Numerical and experimental results at ground plane: profile through front jet pair centerline, $H/D_j = 4$, $U/V_j = 0.09$.

B. Effects of Frame Averaging

At lower velocity ratios, the forward vortex pair merges almost completely with the background in the 127-frame averages of the flowfield, although it is still visible in single frame pictures of the same flowfield. Figure 9 shows a forward vortex pair for U/V_j of 9.03 with the laser sheet two jet diameters above the ground plane. Comparing this figure with Fig. 6 shows that the forward vortex pair becomes much larger at lower forward velocity ratios. In additiion, the location of the forward vortex seems to become much more variable as observed in the movie. This may partially be due to variations in the freestream velocity at such low velocity ratios.

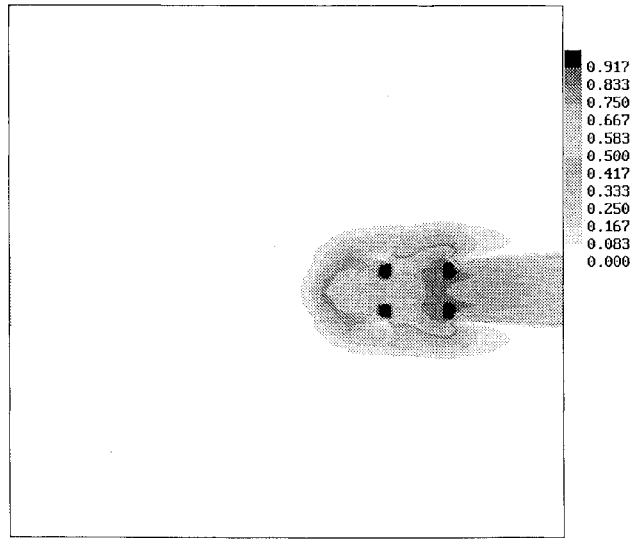

Fig. 17 Numerical temperature profile at body plane: $H/D_j = 4$, $U/V_j = 0.09$.

C. Ground Vortex and Forward Vortex Pair Location Variation

Figure 10 shows the ground vortex location relative to the forward pair of jets as a function of the velocity ratio U/V_j with and without inlet suction, for three different test model heights. At the higher velocity ratios, the ground vortex location appears to be independent of inlet suction and test model height relative to the ground plane. At low velocity ratios, it appears that the ground vortex location depends on the height of the test model above the ground. At greater heights, the inlets have less influence on the location of the ground vortex. Note that the ground vortex location appears to be independent of height with the inlet suction off.

The forward pair location also appears to be influenced by inlet suction. Figure 11 shows the forward vortex location relative to the forward pair of jets as a function of velocity ratio for three different heights. Again, at high velocity ratios the forward vortex location appears to be independent of test model height and inlet suction up to a height of six jet diameters. At low velocity ratios, the distance between the forward vortex pair location and the forward pair of jets appears to increase with increasing height. At lower heights, inlet suction influences considerably the forward vortex pair location. Also, the forward freestream flow contributes less to the overall flowfield in comparison with the inlet suction at lower velocity ratios.

D. Comparison of Numerical and Experimental Results

Comparison of numerical and experimental results with the same geometry and velocities are very similar. Figures 12 and 13 show two contour plots, numerical and experimental data, respectively, near the ground plane for a velocity ratio of 0.09 and a height of four jet diameters. Figure 14 shows profiles through the model centerline of the numerical temperature data and experimental concentration measurements shown in Figs. 12 and 13. Figure 15 shows similar measured and predicted profiles through the jet centerline of the model. Both the experimental concentration measurements and the numerical temperature data have been normalized so that the maximum temperature matches the maximum smoke concentration. Comparison of numerical and experimental data in Fig. 14 shows good agreement, but the profiles through the jet centerlines in Fig. 15 show some differences. In particular, the prediction does not show the high value of concentration that is apparent in experimental data at the location corresponding to that of the forward vortex pair.

Figure 16, a contour plot of numerical and experimental data across the forward pair of jets on the ground plane, shows

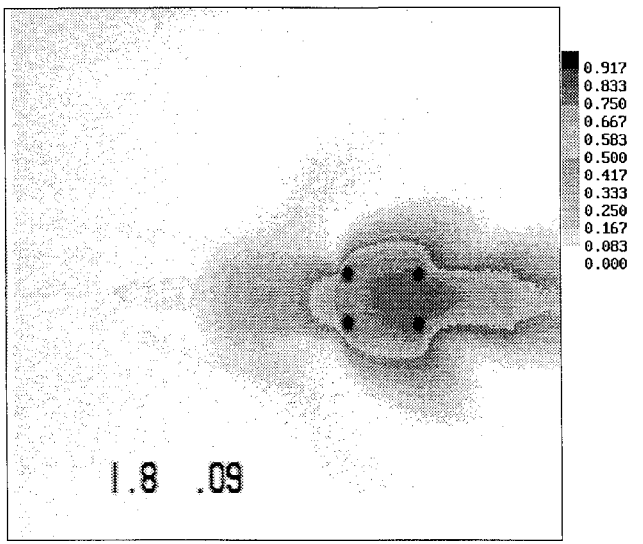

Fig. 18 Experimental smoke concentration at body plane: $H/D_j = 4$, $U/V_j = 0.09$.

that the numerical and experimental data are close except in some areas outside of the jet region.

At the body plane, comparisons of numerical and experimental data are also different, as shown in Figs. 17 and 18. Some of these differences arise from vortex features that are not seen in the numerical data.

IV. Conclusions

The technique presented here has been generally successful in providing quantitative measurements of smoke concentration in a complex flowfield. Data at both short time intervals and time-averaged data can be obtained using this technique. This allows smoke concentration measurements of both turbulent and steady flowfields to be examined. By analogy, smoke concentration can be considered similar to temperature profiles in some applications.

In this experiment, single frame data reveal the clear existence of both asymmetry and turbulence in the flowfield. Single frame data also show a pair of forward vortices. Time-averaged data show a symmetric flowfield, and major flow features such as the forward vortex pair become smeared.

The locations of both the ground vortex and forward vortex pair depend on both the velocity ratio and model height. At high velocity ratios, the distance between the forward pair of jets and the ground vortex and forward vortex pair locations appear to be independent of test model height. Inlet suction does not appear to influence the location of the ground vortex or the forward vortex pair at these high velocity ratios. At low velocity ratios, the distances between the forward pair of jets and the ground vortex and forward vortex pair locations appear to increase with increasing test model height. Inlet suction appears to influence the ground and forward vortex, especially at low model heights. In a large number of these cases, the ground vortex is very near the inlet.

Frame-averaged data sets compare favorably with numerical results in most areas of the flowfield. Individual features, such as the forward vortex pair, may be missed in time-averaged predictions. Mixing in some areas of the flowfield may also be missed in time-averaged predictions. It may be necessary to include several features associated with the instantaneous flow structure for numerical calculations to accurately model such a complex flowfield.

References

[1]Schwantes, E., "The Recirculation Flow Pattern of a VTOL Lift Engine," NASA TT F-14,912, June 1973

[2]Hall, G. R., and Rogers, K. H., "Recirculation Effects Produced by a Pair of Heated Jets Impinging on a Ground Plane," NASA CR-1307, 1969.

[3]Kuhn, Richard E., "The Induced Aerodynamics of Jet and Fan Powered V/STOL Aircraft," *Recent Advances in Aerodynamics*, Springer-Verlag, New York, 1986, pp. 337–373.

[4]MacLean, R. J., "The Flowfield Around a STOVL Aircraft Model in Ground Effect," Master's Thesis, Purdue University, West Lafayette, IN, Aug. 1990.

[5]Bower, W., Saripalli, K., and Agarwal, R., "A Summary of Jet-Impingement Studies at McDonnell Douglas Research Labs," AIAA Paper 81-2613, 1981.

[6]Tafti, D. K., and Vanka, S. P., "The Hot Gas Environment Around STOVL Aircraft in Ground Proximity, Part 2: Numerical Study," AIAA Paper 90-2270, July 1990.

[7]Balint, J. L., Ayrault, M., and Schon, J. P., "Quantitative Investigation of the Velocity and Concentration Fields of Turbulent Flows Combining Visualization and Image Processing," *Flow Visualization III, Proceedings on the Third International Symposium on Flow Visualization*, Hemisphere, Washington, DC, 1983, pp. 254-258.

[8]Morgan, Douglas C., "Concentration Measurements in a Cold Flow Model Annular Combustor Using Laser Induced Fluorescence," Master's Thesis, Purdue University, West Lafayette, IN, Aug. 1988.

[9]VanOverbeke, T. J., and Holdeman, J., "A Numerical Study of the Hot Gas Environment Around a STOVL Aircraft in Ground Proximity," AIAA Paper 88-2882, July 1988.

[10]Colin, F. E., and Olivari, D., "The Impingement of a Circular Jet Normal to a Flat Surface With and Without Crossflow," European Research Office, United States Army Rept. AD-688953, 1969.